

Condensation heat transfer on superhydrophobic surfaces

Nenad Miljkovic and Evelyn N. Wang

Condensation is a phase change phenomenon often encountered in nature, as well as used in industry for applications including power generation, thermal management, desalination, and environmental control. For the past eight decades, researchers have focused on creating surfaces allowing condensed droplets to be easily removed by gravity for enhanced heat transfer performance. Recent advancements in nanofabrication have enabled increased control of surface structuring for the development of superhydrophobic surfaces with even higher droplet mobility and, in some cases, coalescence-induced droplet jumping. Here, we provide a review of new insights gained to tailor superhydrophobic surfaces for enhanced condensation heat transfer considering the role of surface structure, nucleation density, droplet morphology, and droplet dynamics. Furthermore, we identify challenges and new opportunities to advance these surfaces for broad implementation in thermofluidic systems.

Introduction

Vapor condensation is a ubiquitous phenomenon occurring in nature.[1–5] We observe this process in our daily lives, such as on a hot summer day when water accumulates on a cold drink container or on a humid day when fog forms. In industry, vapor condensation is an essential process in power generation,[6] thermal management,[7] water desalination,[8,9] and environmental control.[10] For example, the thermal efficiency of the steam cycle, typically responsible for a major fraction of a nation's power production, is directly linked to condensation heat transfer performance. Meanwhile, in heating, ventilating, and air conditioning (HVAC) systems, which account for ≈20% of the total energy consumption in developed countries,[11] the accumulation of condensed water on thermal components can lead to performance degradation and increased costs. Furthermore, condensation on glass strongly influences the transmittance of light into greenhouses, resulting in a potential 40% decrease in solar energy entering the greenhouse during the winter.[12]

In all of these industrial systems, vapor condenses on a surface rather than directly in the vapor phase due to the reduced energy barrier for droplet nucleation.[13] However, the vapor typically forms a thin liquid film because of the high surface energy of industrial components (i.e., clean metals such as copper, aluminum, stainless steel). While this mode known as filmwise condensation[14] (**Figure 1**a) is quite common, the formation of a liquid film is not desired due to the large resistance to heat transfer. Meanwhile, if a surface is coated with a low-energy non-wetting "promoter" material (i.e., long chain fatty acid, wax, polymer coating, self-assembled monolayer),[15–19] or if it naturally adsorbs hydrocarbons and impurities on its surface from the surroundings (as in the case of gold, silver, and chromium),[20–22] the vapor forms discrete liquid droplets ranging in size from microns to millimeters.[23–25] This process is known as dropwise condensation[26] (Figure 1b). The progressive removal of these condensing droplets by gravity at length scales comparable to the capillary length (≈2.7 mm for water)[27–29] helps refresh the surface for re-nucleation and allows 5–7 times higher heat transfer performance when compared to the filmwise mode.[30]

Since its discovery eight decades ago, dropwise condensation on common heat transfer materials has been a topic of significant interest,[30,31] with a focus on creating non-wetting surfaces via promoter coatings for easy droplet removal. While robust coatings still continue to be a challenge and require more development,[30] recent advancements in nanofabrication have allowed for the development of superhydrophobic surfaces,[32] on which nearly spherical water droplets form with high mobility and minimal droplet adhesion. In addition, the role of surface structuring on wetting characteristics have been studied in detail[33–35] to enhance condensation performance by reducing droplet departure sizes to below that of the capillary

Nenad Miljkovic, Massachusetts Institute of Technology, Cambridge, MA; nmiljkov@mit.edu
Evelyn N. Wang, Massachusetts Institute of Technology, Cambridge, MA; enwang@mit.edu
DOI: 10.1557/mrs.2013.103

© 2013 Materials Research Society

https://doi.org/10.1557/mrs.2013.103 Published online by Cambridge University Press

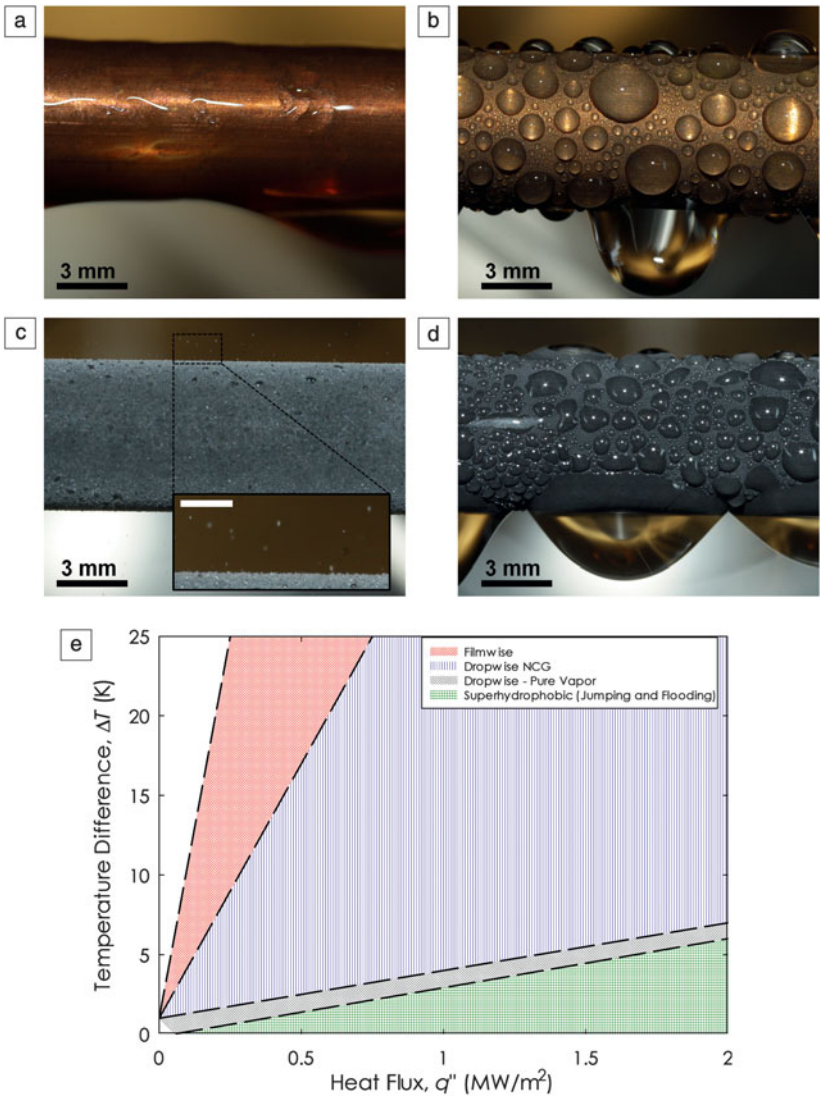


Figure 1. Condensation heat transfer modes and performance. Images of (a) filmwise condensation on a smooth hydrophilic Cu tube, (b) dropwise condensation on a silane coated smooth Cu tube, (c) jumping-droplet superhydrophobic condensation on a nanostructured CuO tube (inset: magnified view of the jumping phenomena, scale bar is 500 μm), and (d) flooding condensation on a nanostructured CuO tube.[47] (e) Heat transfer measurements for dropwise condensation of steam at near-atmospheric pressure[30] ($\Delta T = T_{sat}(P_v) - T_{wall}$). Superhydrophobic region shows expected performance enhancement due to increased droplet mobility. Note: NCG, non-condensable gas; T_{sat}, vapor saturation temperature; P_v, vapor pressure; T_{wall}, condensing surface temperature. Reprinted with permission from Reference 47. © 2013 American Chemical Society.

length (≲3 mm for water) and enabling faster clearing of the surface for re-nucleation.

Yet when small water droplets (≈10–100 μm) merge on suitably designed superhydrophobic surfaces, they can undergo coalescence-induced droplet ejection or "jumping" due to the release of excess surface energy (Figure 1c).[29] Jumping droplet condensation has offered a new avenue to further enhance heat transfer by increasing the time-averaged density of small droplets. However, if the nucleation density is too high and the spacing between droplets is reduced, droplet jumping cannot be sustained. Under such conditions, discrete non-jumping droplets form that are strongly adhered to the surface and can have even worse performance than dropwise condensation, leading to a flooding condensation mode (Figure 1d). The different fluid-surface interactions of the four modes described previously (filmwise, dropwise, jumping, and flooding) accordingly determine the heat transfer performance.

To characterize the condensation performance, the heat flux q'' is a commonly used metric to quantify the amount of latent heat of phase change removed by the surface at a given driving potential. This driving potential is represented by either the temperature difference (ΔT) between the vapor ($T_{sat}(P_v)$) and condensing surface (T_{wall}), $\Delta T = T_{sat}(P_v) - T_{wall}$, or the supersaturation, S, the ratio of the vapor pressure (P_v) to the saturation pressure (P_{sat}) at the surface temperature (T_{wall}), $S = P_v / P_{sat}(T_{wall})$. Accordingly, Figure 1e summarizes the measured (filmwise and dropwise) and expected (jumping and flooding) performance of the four modes, showing q'' with ΔT for steam at atmospheric pressure.[30] If the condensing steam is mixed with non-condensable gases (NCGs) that do not undergo a phase transition during the condensation process (e.g., air), the NCG can accumulate adjacent to the surface, creating an additional diffusional resistance for vapor molecules. The high sensitivity of condensation heat transfer to small amounts (<10 ppm) of air in the steam explains the large range of values and trends shown in Figure 1e for the case of dropwise condensation with NCGs. With the development of superhydrophobic materials, the heat transfer performance should theoretically be able to exceed that of the highest values reported with dropwise condensation. However, due to the complex fluid-surface interactions, the role of structures for enhanced condensation on superhydrophobic surfaces has been unclear until recently, where we have gained new understanding of fluid-surface processes during phase change.

In this article, we review the fabrication, characterization, wettability, and interfacial dynamics of superhydrophobic materials during condensation and discuss insights from recent studies for enhanced heat transfer performance. This article focuses on water as the working fluid due to its favorable heat transfer properties (i.e., high latent heat of vaporization) and its common use in industry. To better understand the physics of the process, we examine the role of surface structure on emerging droplet morphology, nucleation density, droplet

https://doi.org/10.1557/mrs.2013.103 Published online by Cambridge University Press

growth rate, and departure characteristics. Furthermore, we discuss scalable materials for superhydrophobic surfaces with experimentally demonstrated heat transfer performance. Finally, we provide perspectives for the development of next-generation nanostructured materials for enhanced condensation heat transfer.

Condensation physics on superhydrophobic surfaces

Wetting phenomena

We first briefly provide background information related to wetting phenomena to facilitate understanding of condensation on superhydrophobic surfaces. When a droplet is deposited on a smooth surface, it can either wet the surface or form a discrete droplet, depending on the surface energy. Young[36] first proposed that the equilibrium contact angle, θ, of the droplet is dictated by a force balance at the three phase contact line:

$$\cos\theta = \frac{\gamma_{sv} - \gamma_{sl}}{\gamma_{lv}}, \quad (1)$$

where γ_{sv}, γ_{sl}, and γ_{lv} are the solid-vapor, solid-liquid, and liquid-vapor surface tensions, respectively. Continuing the work of Young, Wenzel and Cassie subsequently extended the wetting analysis to rough and porous surfaces. Considering a surface with roughness r, defined by the ratio of the total surface area to the projected area, Wenzel[37] showed that when the fluid wets all of the rough area, the contact angle θ_w is defined by:

$$\cos\theta_w = r\cos\theta. \quad (2)$$

In contrast, Cassie and Baxter[38] considered the case where the droplet rests on the tips of the roughness and showed that the contact angle θ_c is defined by:

$$\cos\theta_c = \varphi(\cos\theta + 1) - 1, \quad (3)$$

where φ is the ratio of the solid area contacting the droplet to the projected area. The two droplet morphologies described in Equations 2 and 3 are termed Wenzel and Cassie, respectively (see the Introductory and Kota et al. article in this issue). Accordingly, in the case of hydrophobic surfaces ($\theta > 90°$), the roughness amplifies the wetting characteristics such that the surface becomes superhydrophobic, where contact angles exceed 150°. While Wenzel and Cassie droplets can both exist on these rough surfaces, the Wenzel state is less desired, owing to the higher adhesion to the substrate compared to the low adhesion Cassie state.[32] As a result, over the past decade, studies have focused on developing superhydrophobic surfaces to limit droplet adhesion and increase water repellency.[32,39–43]

In the case of condensation, however, the nucleation of droplets through the vapor phase can initiate within the roughness, such that Equations 2 and 3 may not apply. Previous studies have shown that on structured superhydrophobic surfaces with well-controlled geometries (defined in **Figure 2**a), highly adhered Wenzel droplets form during vapor condensation, which are distinct from the highly mobile Cassie droplets, which form when liquid is deposited using a syringe.[32,44–46] In fact, three different droplet morphologies exist during condensation, Wenzel (W) (Figure 2a, d), partially wetting (PW) (Figure 2b, e), and suspended (S) (Figure 2c, f), where both S and PW droplets are highly mobile compared to W droplets. Due to the importance of minimizing droplet adhesion, knowledge of the emergent droplet morphology needs to be properly characterized and understood in order to tailor the micro/nanostructured surfaces with controlled roughness (i.e., surface structuring, for enhanced heat transfer).[47]

Structure geometry and nucleation density

Structure geometry and nucleation density have specific roles in the emergent droplet morphology (W, PW, or S). Previous studies have shown that there is a length-scale dependence of the surface structuring (i.e., microstructures[45,48,49] versus nanostructures[29,50–53]) and that global thermodynamic analysis comparing the lower equilibrium energy state (i.e., Cassie versus Wenzel) is insufficient,[40] although often used to explain observed condensation behavior.[45,46,48,49,54] Recently, Enright et al. showed that the morphology of isolated droplets interacting with the surface structures during growth from within a unit cell (volume between structures) is primarily due to (1) energy barriers encountered by the droplet growing within the structured surface (**Figure 3**a), and (2) droplet–droplet interactions governed by the nucleation density (i.e., the average spacing between nucleation sites $\langle L \rangle$ relative to the structure length scale l).[55] Meanwhile, S droplets nucleating on the tips of structures are unconditionally stable, assuming no droplet–droplet interactions and external forces such as gravity.

Enright et al. focused on droplets nucleating within the unit cell because they are more desirable for enhanced heat transfer. Their study showed that these droplets can either grow above the structure forming a "balloon"-like PW droplet (Figure 3b), or laterally spread into the structure forming a highly adhered W droplet (Figure 3c).[54,55] While the droplet morphology is dictated by the intricate liquid/structure interaction dynamics, it can be approximately predicted by comparing the energies of the non-equilibrium advancing Cassie and Wenzel states with a dimensionless energy ratio:

$$E^* = \frac{\cos\theta_{A,c}}{\cos\theta_{A,w}} = \frac{-1}{r\cos\theta_A}, \quad (4)$$

where $r = 1 + \pi dh/l^2$ is the surface roughness, d is the structure width/thickness, h is the structure height, l is the center-to-center distance between adjacent structures, and θ_A is the advancing contact angle on a flat surface. Equation 4 implies that when $E^* > 1$, W droplet morphologies are favored, while when $E^* < 1$, PW droplets should emerge.[55] In addition to this energy criterion, the nuclei of the droplets need to be 2–5 times the spacing between the structures (Figure 3d) ($\langle L \rangle / l > 2–5$). If droplets grow and merge too close to each other such that $\langle L \rangle / l < 2–5$, coalescence events bypass the energy barrier associated with individual droplet growth (Equation 4) and flood the surface, forming undesired highly adhered W droplets (Figure 3e). Accordingly, a regime map defining the

https://doi.org/10.1557/mrs.2013.103 Published online by Cambridge University Press

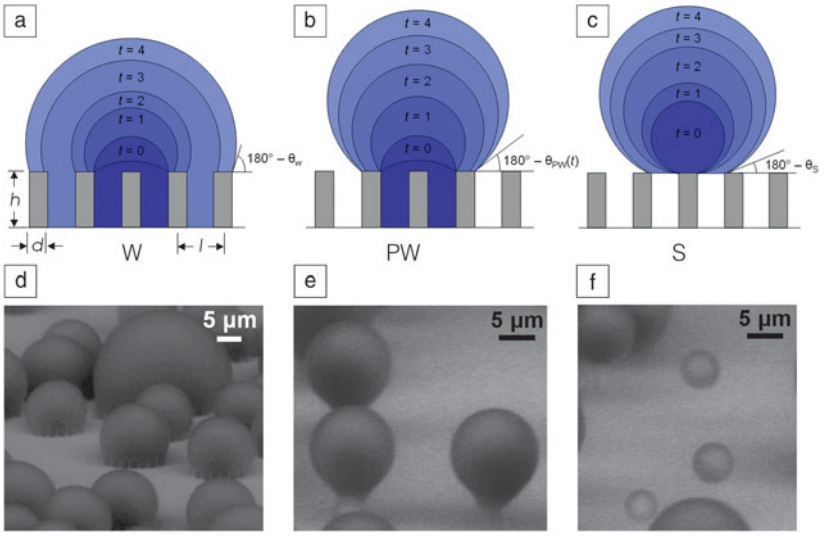


Figure 2. Condensing droplet morphologies. Time-lapse schematics of a (a) Wenzel (W) droplet where liquid fills the structures beneath the droplet; (b) partially wetting (PW) droplet where the liquid partially fills the structure beneath the droplet, and (c) suspended (S) droplet where an air layer fills the structure beneath the droplet[84] (schematics not to scale). Environmental scanning electron microscopy[120–130] images of droplets with the (d) W, (e) PW, and (f) S morphologies on a nanostructured surface (h = 6.1 μm, l = 2 μm, d = 300 nm). Note: t, time; θ_w, Wenzel droplet contact angle (Equation 2); θ_{pw}, partially wetting contact angle; θ_s, suspended droplet contact angle. Reprinted with permission from Reference 84. © 2013 American Society of Mechanical Engineers.

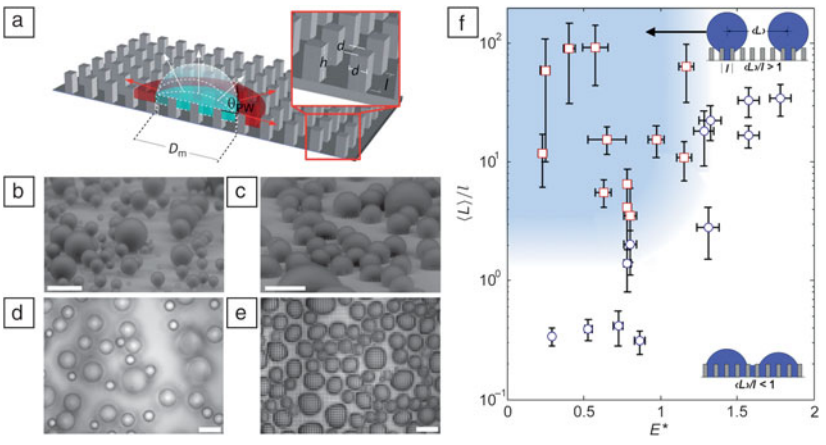


Figure 3. Effect of structure length scale and nucleation density on emergent droplet morphology. (a) Schematic of a droplet growing within the confines of the structures. The liquid can either grow laterally by filling the adjacent structures or by growing upward above the structures.[54] Condensed droplet growth observed using environmental scanning electron microscopy on structured surfaces with (b) Cassie droplets, where l = 2 μm, and (c) Wenzel droplets, where l = 4 μm.[55] Scale bar for (b, c) is 60 μm. Condensation behavior on a microstructured surface (l = 4.5 μm, d = 2 μm, h = 5 μm, and E^* = 0.75 ± 0.04) is shown at a fixed location with a scaled coalescence length of (d) $\langle L\rangle/l$ = 3.54 ± 2.43 (PW droplets) and (e) $\langle L\rangle/l$ = 2.04 ± 0.6 (W droplets).[55] Scale bar for (d, e) is 50 μm. (f) Regime map characterizing the dominant wetting behavior observed during condensation with coordinates of $\langle L\rangle/l$ and E^*. PW morphologies (red □) emerge at large $\langle L\rangle/l$ and $E^* \lesssim 1$ (shaded region). Wenzel morphologies (blue ○) emerge at low $\langle L\rangle/l$ and/or $E^* \gtrsim 1$.[55] Note: E^*, dimensionless energy ratio; θ_{PW}, advancing contact angle; D_m, wetted basal diameter; $\langle L\rangle$, average distance between droplet nucleation sites. Adapted with permission from Reference 55. © 2013 American Chemical Society, and Reference 54. © 2012 Royal Society of Chemistry.

parametric space with experimentally measured $\langle L\rangle/l$ ratios and calculated E^* in Figure 3f determines the emergent droplet morphology for a wide variety of structure length scales, geometries, and nucleation densities. The results suggest that an important aspect is defining the location of, and distance between, nucleation sites to favor formation of highly mobile PW droplet morphologies.

Tailoring surface chemistry for nucleation

Controlling nucleation has been investigated but has primarily focused on patterning surface chemistry heterogeneities[56–62] (hybrid hydrophobic/hydrophilic surfaces) at the length scale of the structures or larger to simultaneously increase the nucleation rate (hydrophilic spots) and achieve high droplet mobility (hydrophobic spots). Although spatial control of nucleation has been demonstrated,[58] it was also accompanied by higher droplet adhesion.[63] The hydrophilic spots on the surface act to pin the droplet and result in slower removal.[30] However, S droplets with low adhesion were obtained using hybrid surfaces by ensuring that the height-to-thickness ratio of the structures (i.e., with pillars having hydrophilic tops and hydrophobic valleys) is relatively large (>2).[63] Therefore, with proper design, hybrid surfaces have the potential to enhance droplet shedding for enhanced condensation while controlling nucleation density.

To define the location of nucleation sites at length scales smaller than the structure (<10 nm), in order to delay flooding condensation, Enright et al.[55] showed that defects (i.e., spots of incomplete coverage) in the hydrophobic coatings exist,[64–66] which with the proper structure geometry can be used to determine the formation of highly mobile PW and S droplets. Hydrophobic coatings with tailored defects present an opportunity to control droplet morphology while further enhancing heat transfer.

Effect of droplet morphology on growth dynamics

While both PW and S droplets show advantages in terms of easy droplet removal as opposed to W droplets, droplet growth prior to departure needs to be considered to determine the desired morphology for enhanced heat transfer. Miljkovic et al.[67] highlighted the importance of considering droplet morphology on growth

https://doi.org/10.1557/mrs.2013.103 Published online by Cambridge University Press

rates, whereby in certain cases, surface structuring can degrade heat transfer performance. Using a specific structure geometry, they demonstrated that the growth rate (**Figure 4**a–b) and individual droplet heat transfer of PW droplets were 6 and 4–6 times higher than that of S droplets, respectively. This difference was due to the fact that S droplets are suspended on top of a composite air-solid interface, where the air adds significant thermal resistance for droplet growth. To investigate the effect of the morphology on overall surface heat transfer, a thermal-resistance-based droplet growth model was developed[67–71] (Figure 4c), and it was demonstrated that surfaces favoring only S droplet formation degraded the overall heat transfer coefficient by 71% when compared to flat hydrophobic shedding surfaces, despite their high mobility.[67] The study showed that structure design needs to be carefully considered to minimize the effect of the air beneath the droplet, while maintaining easy droplet removal. Accordingly, this thermal resistance can be decreased by reducing the structure heights via nanoscale roughness.

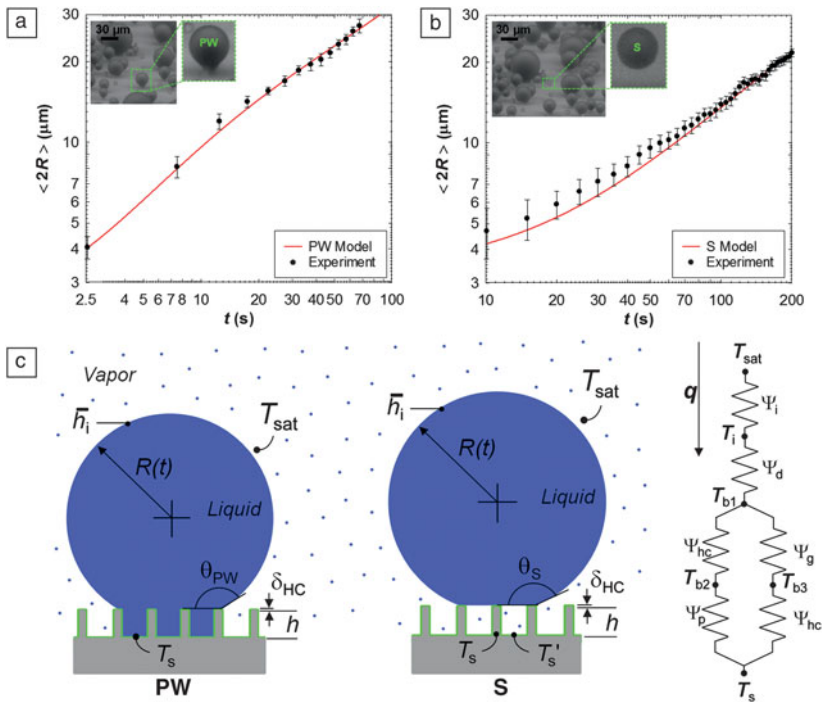


Figure 4. Effect of droplet morphology on growth rate. Time evolution of the average droplet diameter for (a) partially wetting (PW) and (b) suspended (S) droplets (h = 6.1 μm, l = 2 μm, d = 300 nm). The S droplet had a slower growth rate than the PW droplet due to poor thermal contact between the base and substrate.[67] (c) PW and S droplet model schematics and thermal resistance diagram showing the liquid-vapor interface (Ψ_i), droplet conduction (Ψ_d), hydrophobic coating (Ψ_{hc}), pillar (Ψ_p), and gap (Ψ_g) thermal resistances.[67] Note: t, time; T_s, substrate temperature at the base of a pillar; T_s', substrate temperature in between two adjacent pillars; h, pillar height; $\bar{h}_i$, interfacial heat transfer coefficient; T_{sat}, vapor saturation temperature; $R(t)$, droplet radius as a function of time; T_i, liquid-vapor interface temperature; T_{b1}, hydrophobic coating surface temperature on the tips of the pillars; T_{b2}, pillar/hydrophobic coating interface temperature; T_{b3}, hydrophobic coating surface temperature in the valleys of the pillars; q, individual droplet heat transfer rate; δ_{hc}, hydrophobic coating thickness; θ_S, suspended droplet contact angle; θ_{PW}, partially wetting droplet contact angle. Reprinted with permission from Reference 67. © 2012 American Chemical Society.

To tailor the emergent droplet morphology, Miljkovic et al.[47] suggested a method to favor PW droplet formation via the creation of thermodynamic energy barriers for nucleation on structure tips.[72] By making the tip thickness comparable to the critical nucleation radius (≈10–30 nm for water), the energy barrier for nucleation on the tip is increased, resulting in favorable droplet nucleation within the structure and stable formation of PW droplets.[47] It is important to note that this approach is valid, assuming the nucleation density of droplets is low compared to the density of the structures ($\langle L \rangle / l > 2-5$) such that flooding is avoided (Figure 3f).

Droplet departure

Once the droplets nucleate and grow with the desired morphology, droplets also need to be quickly removed from the surface to enhance heat transfer.[73] Recent work by Boreyko et al.[29] and Narhe et al.[74] present a new method for efficient droplet departure, whereby in contrast to gravitational shedding on a smooth hydrophobic surface (**Figure 5**a), condensate droplets spontaneously jump on a superhydrophobic surface without any external forces (Figure 5b). The average droplet radius at steady state was 30 times smaller than the capillary length (≈2.7 mm for water), and therefore promises significant heat transfer improvement due to the smaller time-averaged distribution of droplets.[75] The spontaneous motion is powered by the surface energy released upon droplet coalescence and the out-of-plane jumping results from in-plane coalescence (Figure 5c–d). While both PW and S droplet morphologies are capable of jumping at equivalent length scales,[76] as discussed earlier, PW droplets are favored due to their higher growth rates.[67] It is important to note, if the solid fraction of the structure is too large ($\varphi \geq 0.1$), PW and S droplet jumping may not be possible due to high adhesion.

To achieve droplet jumping, surface structures need to be designed with minimal droplet adhesion by using nanoscale structures with low solid fractions ($\varphi < 0.1$), or hierarchical structures[77–81] (consisting of a dual length scale roughness of micro- and nanostructure). Extending the work of Boreyko, many researchers have modeled[76,82–84] and fabricated[50,52,85–89] surfaces that show stable droplet jumping. However, if the supersaturation is too large (high nucleation density), flooding occurs, and droplets are formed that strongly adhere to the surface.[47,55] These nucleation density limitations still remain and need to be addressed to further increase the operating range of superhydrophobic surfaces. Furthermore, heat transfer measurements are required to better quantify the condensation

https://doi.org/10.1557/mrs.2013.103 Published online by Cambridge University Press

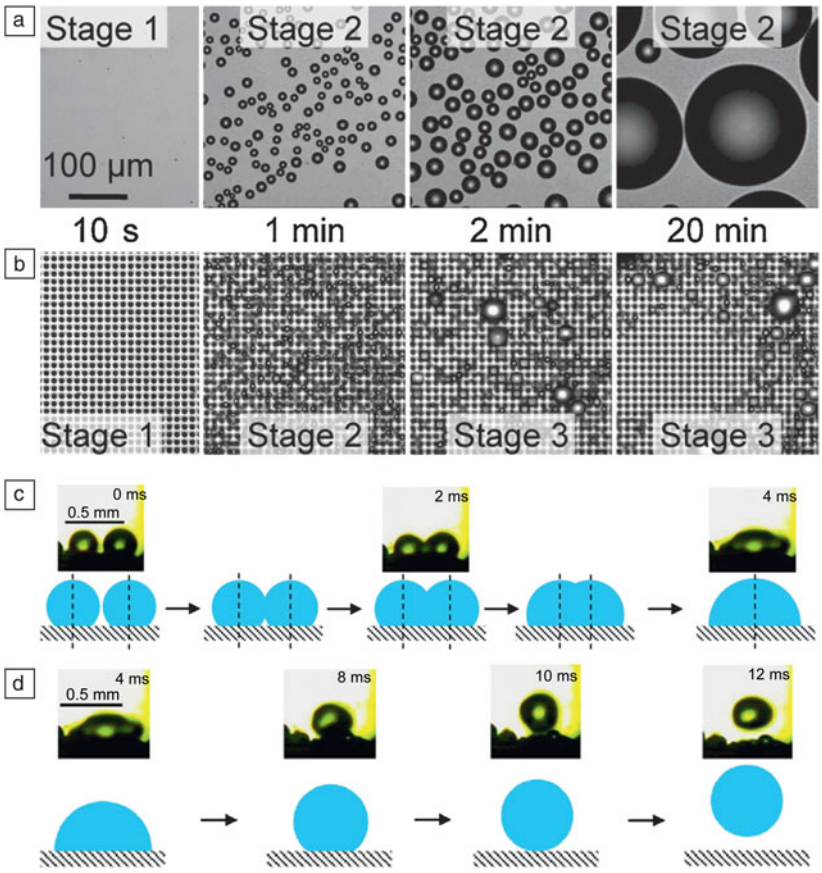


Figure 5. Droplet departure modes—gravitational shedding versus jumping. Dropwise condensation on a horizontally oriented (a) smooth hydrophobic surface and (b) structured two-tier superhydrophobic surface (with micro-pillars visible). Stages 1–3 of the condensation process characterize the initial nucleation, immobile coalescence, and mobile coalescence (jumping droplets), respectively.[29] (c) Coalescing process of two droplets. Upper photos: side-view images of two condensed drops with diameters of 302 and 252 μm during merging; lower: modeled coalescence process.[83] (d) Coalescence-induced transformation and jumping of the merged droplet. Upper photos: side-view images of coalescence-induced droplet jumping; lower: modeled coalescence-induced droplet jumping.[83] Reprinted with permission from Reference 29. © 2009 The American Physical Society, and Reference 83. © 2012 Elsevier.

enhancement when compared to state-of-the-art dropwise condensing surfaces.

Condensation heat transfer performance on superhydrophobic surfaces

Modeling of enhanced superhydrophobic surfaces

As shown by previous studies, condensation heat transfer performance on superhydrophobic surfaces is dependent on many factors, including droplet morphology, structure geometry, and departure dynamics. To obtain design guidelines for enhanced condensation heat transfer with superhydrophobic structured surfaces, Miljkovic et al.[84] developed a unified model coupling individual droplet heat transfer, droplet size distribution, and droplet wetting morphology. The emergent droplet wetting morphologies, PW and S jumping, PW and S non-jumping, or W, were determined by coupling the structure geometry with the nucleation density and considering local energy barriers to wetting. The model results suggest that a specific range of geometries (0.5–2 μm) and nucleation densities allow for the formation of coalescence-induced PW jumping droplets with a promise of 190% overall surface heat flux enhancement over conventional flat dropwise condensing surfaces.[84]

Fabrication of scalable nanostructures

While a considerable amount of work has focused on understanding and fabricating superhydrophobic surfaces for potential enhancements in condensation,[29,52,54,67,68,74,75,86–90] heat transfer measurements that quantify the improvement in performance using these surfaces are limited. In addition, many studies have used well-defined structures to facilitate our understanding of the condensation process (carbon nanotubes,[53] nanowires,[54] nanoparticle self-assembly,[91] micropillars[55,58]); however, it is also important to pursue scalable methods of fabricating superhydrophobic surfaces for the implementation in large-scale thermal applications.

Recently, researchers have proposed metal oxides to fabricate more scalable superhydrophobic nanostructured surfaces.[47,85,86,92–97] The nanoscale oxide can (1) better satisfy the requirement for the structure density to be larger than the nucleation density in order to avoid flooding,[55] and (2) reduce the structure length scale beneath the droplet in order to minimize the structure thermal resistance.[67]

The works of Miljkovic et al.[47] (**Figure 6**a–c), Feng et al.,[85,94] and Torresin et al.[93] (Figure 6d–f) studied scalable functionalized copper oxide (CuO) nanostructured surfaces. Copper is a typical heat exchanger material where chemical-oxidation based CuO nanostructuring allows for self-limiting growth behavior, resulting in a low characteristic oxide structure height ($h \approx 1$ μm) and a low parasitic conduction thermal resistance.[98,99] From an industrial perspective, the CuO fabrication method is appealing because it can be applied to arbitrarily shaped surfaces, where the nanostructures form at low temperatures and do not require any high temperature annealing or drying processes. While zinc oxide (ZnO) has also been proposed where Narhe et al.[92] showed that the ZnO nanostructures had a favorable morphology (Figure 6g–i), researchers were not able to achieve droplet jumping due to incomplete hydrophobic coating coverage, relatively large solid fractions $\varphi \approx 0.11$, and subsequently larger droplet adhesion to the surface. Furthermore, in addition to copper and zinc oxides, opportunities remain to create scalable nanostructured superhydrophobic

https://doi.org/10.1557/mrs.2013.103 Published online by Cambridge University Press

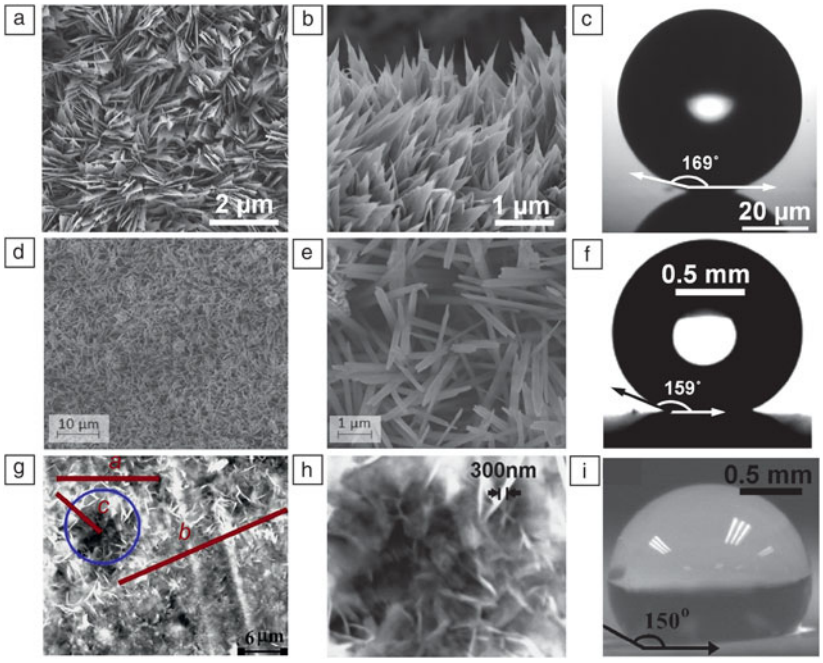


Figure 6. Fabricated scalable nanostructured surfaces. Field emission scanning electron microscopy images of a CuO nanostructured surface with (a) top view, (b) side view, and (c) micro-goniometer contact angle measurement after hydrophobic functionalization (θ_A = 169.2 ± 3°). Nanostructured CuO was formed by immersing the cleaned copper into a hot (96 ± 3°C) alkaline solution composed of $NaClO_2$, NaOH, $Na_3PO_4{\cdot}12H_2O$, and DI water (3.75:5:10:100 wt%). The sharp, knife-like CuO structures have characteristic heights, $h \approx 1$ μm, solid fraction, $\varphi \approx 0.023$, and roughness factor, $r \approx 10$.[47] (d, e) Scanning electron microscopy (SEM) images of the copper surface structures fabricated via wet chemistry by immersing clean copper into a mixture solution containing 2.5 mol/L NaOH and 0.1 mol/L $(NH_4)_2S_2O_8$ at room temperature for 12 min.[93] (f) Contact angle measurement on functionalized nanostructured copper surface (5 μL droplet, θ_A = 159 ± 2°).[93] (g) SEM images of a nanostructured zinc surface showing a micro-flower-like structure (size, $a \approx 12$ μm; separation, $b \approx 25$ μm; height $c \approx 10$ μm).[92] Nanostructured zinc was formed by immersing the zinc substrate in 2 mol/L urea solution prepared with deionized water and *N*-*N*-dimethylformamide in 2:1 volume ratio, in a sealed bottle and kept at 80°C for 20–24 hours. (h) The micro-flower area inside the circle in (g) at large magnification. It shows nano-sheets with an average thickness of 300 nm.[92] (i) Contact angle measurement of a 3 μl water droplet on the ZnO surface. All three scalable surfaces showed high degrees of superhydrophobicity (c, f, and i), promising potential for enhanced condensation heat transfer performance. Reprinted with permission from References 47 and 93. © 2013 American Chemical Society, and Reference 92. © 2010 Elsevier.

surfaces with aluminum and stainless steel, which are commonly used industrial heat exchanger materials.[30]

Heat transfer experiments

An important metric for optimized superhydrophobic surfaces for condensation is experimental heat transfer measurements, however, it is well-known that accurate results are difficult to obtain. Due to the high sensitivity to the presence of NCGs, experiments need to be performed in controlled environments to ensure NCG content of <0.25%.[30,100] In addition, the thermal contact resistance (i.e., the resistance to heat flow at the interface between two bodies in contact) between the sample substrate and test rig have led to a lack of repeatability in heat transfer measurements. Recently, a few studies have conducted experimental investigations in pure vapor environments (no NCGs).[47,93,101–103] The first performance measurement was achieved by Boreyko et al.[101] via the characterization of a jumping droplet thermal diode (**Figure 7**a), which allowed heat to preferentially flow in one direction compared to the other. Although indirect (condensation and evaporation performance were lumped together), the results showed forward effective thermal conductivities of 350 W/mK (Figure 7b), while the reverse thermal conductivity was estimated to be 0.29 W/mK, indicating that the jumping droplet mechanism enhanced heat transfer.

To specifically quantify condensation heat transfer performance, Miljkovic et al.[47] tested superhydrophobic nanostructured CuO tube surfaces (Figure 7c) over a range of supersaturations ($1.02 < S < 1.6$). They demonstrated (Figure 7d) that in the jumping regime, where $S < 1.12$, heat transfer coefficients were $\bar{h}_{jumping} \approx$ 92 kW/m^{2}K (green ★), 30% higher than that of state-of-the-art dropwise condensing copper surfaces (orange ■). However, at $S > 1.12$, flooding degraded performance to $\bar{h}_{flooded} \approx$ 44 kW/m^{2}K (blue □), 41% less than that of copper. Other studies have also observed flooding on two-tier superhydrophobic carbon nanotube[101] and nanostructured CuO[93] surfaces, due to high nucleation densities compared to the structure density (Figure 3f), consequently underperforming compared to dropwise condensation.

Although the results show potential for efficient droplet jumping heat transfer enhancement, the flooding observed by many researchers suggests the need to further reduce the structure length scale and/or reduce and control the nucleation density at elevated supersaturations.

Summary and future outlook

Superhydrophobic surfaces for enhanced condensation require the careful control of surface structure length scale and geometry, nucleation density, droplet morphology, and departure dynamics. Currently, metal oxides are one of the most promising materials to create these superhydrophobic surfaces in a scalable manner due to their ability to form partially wetting droplets, their relatively large thermal conductivities, reduced structure length scales, and low droplet adhesion for stable droplet jumping. In addition, jumping condensation has the potential to enhance heat transfer in the presence of noncondensable gases[104–106] via boundary layer mixing, in addition to the 30% enhancement already observed in pure vapor environments. However, these surfaces remain limited due to flooding for applications with low supersaturations. In the

https://doi.org/10.1557/mrs.2013.103 Published online by Cambridge University Press

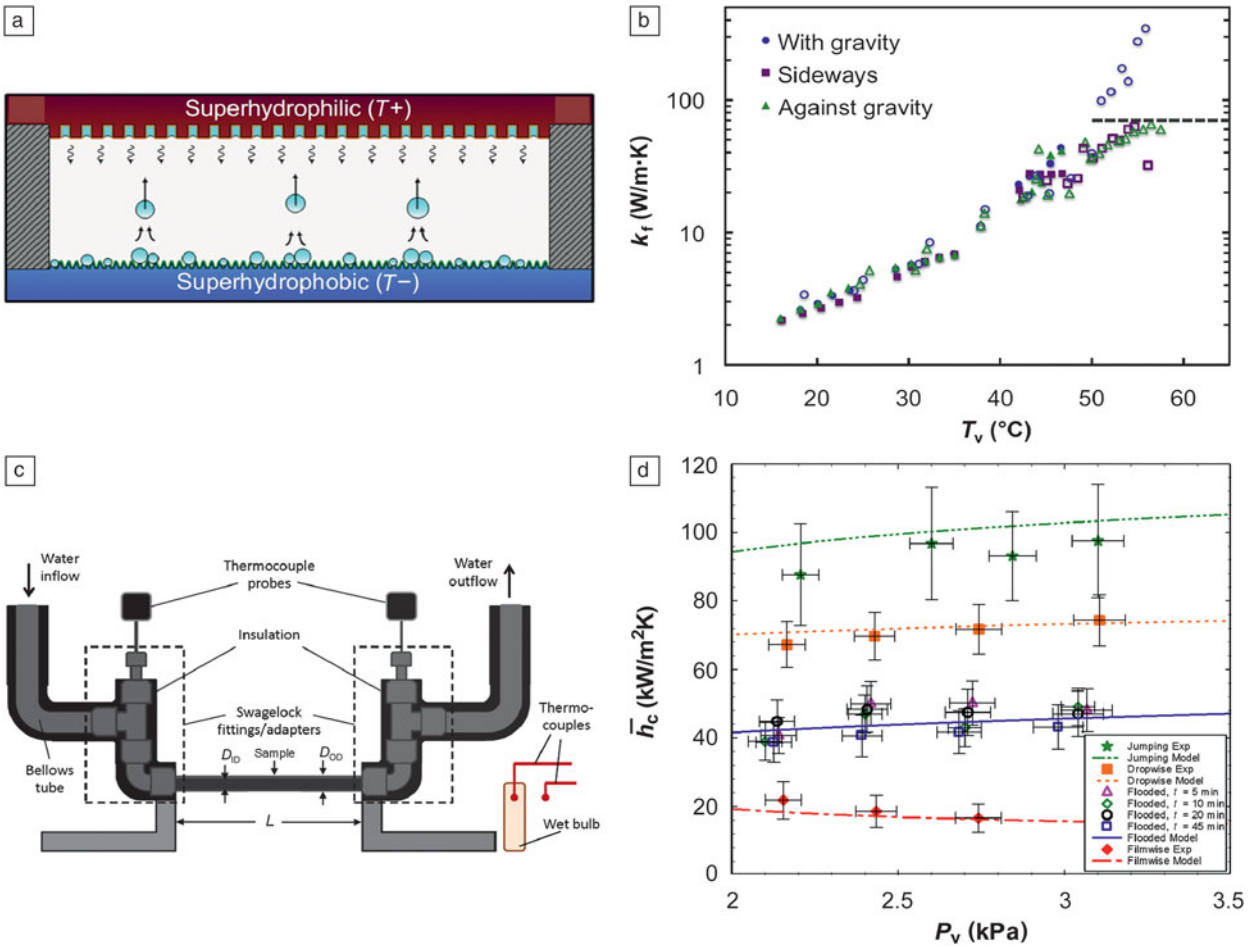


Figure 7. Experimental heat transfer results. (a) Schematic of the planar jumping-droplet thermal diode (not to scale) in forward mode with jumping droplets returning the working fluid from the low temperature (*T*-) superhydrophobic condenser to the high temperature (*T*+) superhydrophilic evaporator for continuous phase-change heat transfer.[101] (b) Forward thermal conductivity (k_f) versus the average vapor temperature of the thermal diode (T_v). For all three orientations tested (sideways, with gravity, and against gravity), the thermal diode performance was the same, highlighting the advantageous orientation independence of condensers having jumping droplet departure.[101] At higher vapor temperatures (T_v > 50°C), boiling in the evaporator was initiated, resulting in orientation dependence (dotted line). (c) Schematic showing setup for condensation experiments. The tube sample (D_{OD} = outer diameter = 6.35 mm, D_{ID} = inner diameter = 3.56 mm, *L* = length = 131 mm) was cooled via chilled water flowing inside the tube at 5 ± 0.1 L/min.[47] (d) Experimental and theoretical steady-state condensation coefficient ($\bar{h}_c$) as a function of saturated vapor pressure (P_v) for tube surfaces shown in (c) undergoing filmwise, dropwise, flooding (four different chemical oxidation times, *t* = 5, 10, 20, and 45 min), and jumping (*t* = 10 min) condensation.[47] Jumping condensation shows the highest condensation heat transfer coefficient for low supersaturations (*S* < 1.12).[47] Adapted with permission from Reference 101. © 2012 American Institute of Physics, and Reference 47. © 2013 American Chemical Society.

future, control of nucleation density through the creation of coatings and using deposition methods for the inclusion of well-defined defects at the molecular scale and minimization of the structure length scale are promising pathways to extend the operating limits. Furthermore, significant efforts should be expended on creating robust hydrophobic coatings at high temperatures. As in classical dropwise condensation, the degradation of the hydrophobic coating poses significant challenges for industrial implementation. One idea showing promise is the study and formation of naturally occurring hydrophobic materials, such as ceramics.[107,108]

A second avenue for future research is with structured surfaces infused with a lubricating fluid (i.e., slippery liquid-infused porous surface [SLIPS], to reduce droplet adhesion) (see the Introductory article in this issue).[109,110] SLIPS provides an alternative approach for further performance enhancement at larger supersaturations,[111] eliminating flooding of the surface structure while maintaining low droplet adhesion.[112–115] In addition, the ability of these surfaces to be omniphobic[116–119] or superamphiphobic allows for their potential use in applications involving low surface tension nonpolar fluids such as refrigerants, where superhydrophobic surfaces can no longer achieve non-wetting behavior. Although promising, further studies into the robustness of SLIPS under industrial conditions, as well as their longevity, are needed in addition to experimental demonstration of heat transfer performance. While limitations

https://doi.org/10.1557/mrs.2013.103 Published online by Cambridge University Press

exist, progress in the area of superhydrophobic surfaces for enhanced heat transfer has been considerable, deepening our fundamental knowledge, introducing new scalable fabrication techniques, and setting new benchmarks for heat transfer performance. Further advances in creating and tailoring robust nanostructures and hydrophobic coatings promise to one day make superhydrophobic surfaces the material of choice for high heat flux condensation applications.

Acknowledgments

We gratefully acknowledge funding support from the MIT S3TEC Center, an Energy Frontier Research Center funded by the Department of Energy, Office of Science, Office of Basic Energy Sciences, Office of Naval Research Young Investigator Award, and Air Force Office of Scientific Research Young Investigator Award.

References

1. A.R. Parker, C.R. Lawrence, *Nature* **414**, 33 (2001).
2. Y.M. Zheng, H. Bai, Z.B. Huang, X.L. Tian, F.Q. Nie, Y. Zhao, J. Zhai, L. Jiang, *Nature* **463**, 640 (2010).
3. B. Bhushan, *Philos. Trans. R. Soc. London, Ser. A* **367**, 1445 (2009).
4. Y.T. Cheng, D.E. Rodak, *Appl. Phys. Lett.* **86** (2005).
5. B. Mockenhaupt, H.J. Ensikat, M. Spaeth, W. Barthlott, *Langmuir* **24**, 13591 (2008).
6. J.M. Beer, *Prog. Energy Combust. Sci.* **33**, 107 (2007).
7. T.B. Peters, M. McCarthy, J. Allison, F.A. Dominguez-Espinosa, D. Jenicek, H.A. Kariya, W.L. Staats, J.G. Brisson, J.H. Lang, E.N. Wang, *IEEE Trans. Compon. Packag. Manuf. Technol.* **2**, 1637 (2012).
8. A.D. Khawaji, I.K. Kutubkhanah, J.M. Wie, *Desalination* **221**, 47 (2008).
9. T. Humplik, J. Lee, S.C. O'Hern, B.A. Fellman, M.A. Baig, S.F. Hassan, M.A. Atieh, F. Rahman, T. Laoui, R. Karnik, E.N. Wang, *Nanotechnology* **22**, 292001 (2011).
10. L. Perez-Lombard, J. Ortiz, C. Pout, *Energy Build* **40**, 394 (2008).
11. B.Z. Li, R.M. Yao, *Renewable Energy* **34**, 1994 (2009).
12. B. von Elsner, D. Briassoulis, D. Waaijenberg, A. Mistriotis, C. von Zabeltitz, J. Gratraud, G. Russo, R. Suay-Cortes, *J. Agric. Eng. Res.* **75**, 1 (2000).
13. D. Kaschiev, *Nucleation: Basic Theory With Applications* (Butterworth-Heinemann, Oxford, 2000).
14. W.Z. Nusselt, *Z. Ver. Dtsch. Ing.* **60**, 541 (1916).
15. P.J. Marto, D.J. Looney, J.W. Rose, A.S. Wanniarachchi, *Int. J. Heat Mass Trans.* **29**, 1109 (1986).
16. R.W.I. Bonner, in *Proceedings of the International Heat Transfer Conference* (ASME, Washington, DC, 2010).
17. S. Vemuri, K.J. Kim, B.D. Wood, S. Govindaraju, T.W. Bell, *Appl. Therm. Eng.* **26**, 421 (2006).
18. S. Vemuri, K.J. Kim, *Int. J. Heat Mass Trans.* **49**, 649 (2006).
19. A.K. Das, H.P. Kilty, P.J. Marto, G.B. Andeen, A. Kumar, *J. Heat Trans.* **122**, 278 (2000).
20. R.A. Erb, E. Thelen, *Ind. Eng. Chem.* **57**, 49 (1965).
21. D.G. Wilkins, L.A. Bromley, S.M. Read, *AIChE J.* **19**, 119 (1973).
22. D.W. Woodruff, J.W. Westwater, *Int. J. Heat Mass Trans.* **22**, 629 (1979).
23. D. Beysens, *C.R. Phys.* **7**, 1082 (2006).
24. D. Beysens, A. Steyer, P. Guenoun, D. Fritter, C.M. Knobler, *Phase Transitions* **31**, 219 (1991).
25. D. Fritter, C.M. Knobler, D.A. Beysens, *Phys. Rev. A* **43**, 2858 (1991).
26. E. Schmidt, W. Schurig, W. Sellschopp, *Forsch. Ingenieurwes.* **1**, 53 (1930).
27. H.Y. Kim, H.J. Lee, B.H. Kang, *J. Colloid Interface Sci.* **247**, 372 (2002).
28. P. Dimitrakopoulos, J.J.L. Higdon, *J. Fluid Mech.* 395, **181** (1999).
29. J.B. Boreyko, C.H. Chen, *Phys. Rev. Lett.* **103**, 184501 (2009).
30. J.W. Rose, *Proc. Inst. Mech. Eng., Part A: J. Power Eng.* **216**, 115 (2002).
31. B.S. Sikarwar, S. Khandekar, S. Agrawal, S. Kumar, K. Muralidhar, *Heat Trans. Eng.* **33**, 301 (2012).
32. A. Lafuma, D. Quéré, *Nat. Mater.* **2**, 457 (2003).
33. N.A. Patankar, *Soft Matter* **6**, 1613 (2010).
34. L. Bocquet, E. Lauga, *Nat. Mater.* **10**, 334 (2011).
35. S.H. Kang, N. Wu, A. Grinthal, J. Aizenberg, *Phys. Rev. Lett.* **107**, 177802 (2011).
36. T. Young, *Philos. Trans. R. Soc. London* **95**, 65 (1805).
37. R.N. Wenzel, *Ind. Eng. Chem.* **28**, 988 (1936).
38. A.B.D. Cassie, S. Baxter, *Trans. Faraday Soc.* **40**, 546 (1944).
39. L.C. Gao, A.Y. Fadeev, T.J. McCarthy, *MRS Bull.* **33**, 747 (2008).
40. D. Quéré, *Annu. Rev. Mater. Res.* **38**, 71 (2008).
41. C. Dorrer, J. Ruhe, *Soft Matter* **5**, 51 (2009).
42. P. Roach, N.J. Shirtcliffe, M.I. Newton, *Soft Matter* **4**, 224 (2008).
43. S. Moulinet, D. Bartolo, *Eur. Phys. J. E* **24**, 251 (2007).
44. R.D. Narhe, D.A. Beysens, *Europhys. Lett.* **75**, 98 (2006).
45. R.D. Narhe, D.A. Beysens, *Phys. Rev. Lett.* **93**, 076103 (2004).
46. R.D. Narhe, D.A. Beysens, *Langmuir* **23**, 6486 (2007).
47. N. Miljkovic, R. Enright, Y. Nam, K. Lopez, N. Dou, J. Sack, E.N. Wang, *Nano Lett.* **13**, 179 (2013).
48. C. Dorrer, J. Ruhe, *Langmuir* **23**, 3820 (2007).
49. K.A. Wier, T.J. McCarthy, *Langmuir* **22**, 2433 (2006).
50. C.H. Chen, Q.J. Cai, C.L. Tsai, C.L. Chen, G.Y. Xiong, Y. Yu, Z. Ren, *Appl. Phys. Lett.* **90**, 173108 (2007).
51. C. Dorrer, J. Ruhe, *Adv. Mater.* **20**, 159 (2008).
52. X. Chen, J. Wu, R. Ma, M. Hua, N. Koratkar, S. Yao, Z. Wang, *Adv. Funct. Mater.* **21**, 4617 (2011).
53. K.K.S. Lau, J. Bico, K.B.K. Teo, M. Chhowalla, G.A.J. Amaratunga, W.I. Milne, G.H. McKinley, K.K. Gleason, *Nano Lett.* **3**, 1701 (2003).
54. K. Rykaczewski, W.A. Osborn, J. Chinn, M.L. Walker, J.H.J. Scott, W. Jones, C. Hao, S. Yaod, Z. Wang, *Soft Matter* **8**, 8786 (2012).
55. R. Enright, N. Miljkovic, A. Al-Obeidi, C.V. Thompson, E.N. Wang, *Langmuir* **40**, 14424 (2012).
56. D.M. Anderson, M.K. Gupta, A.A. Voevodin, C.N. Hunter, S.A. Putnam, V.V. Tsukruk, A.G. Fedorov, *ACS Nano* **6**, 3262 (2012).
57. K.K. Varanasi, T. Deng, in *12th IEEE Intersociety Conference on Thermal and Thermomechanical Phenomena in Electronic Systems* 1–5 (Los Vegas, NV, 2010).
58. K.K. Varanasi, M. Hsu, N. Bhate, W.S. Yang, T. Deng, *Appl. Phys. Lett.* **95**, 094101 (2009).
59. E.K. Her, T.J. Ko, K.R. Lee, K.H. Oh, M.W. Moon, *Nanoscale* **4**, 2900 (2012).
60. S.M. Ji, I.Y. Kim, E.H. Kim, J.U. Jung, W.D. Kim, H.E. Lim, *J. Korean Soc. Precis. Eng.* **29**, 19 (2012).
61. A. Lee, M.W. Moon, H. Lim, W.D. Kim, H.Y. Kim, *Langmuir* **28**, 10183 (2012).
62. S.C. Thickett, C. Neto, A.T. Harris, *Adv. Mater.* **23**, 3718 (2011).
63. C.W. Yao, T.P. Garvin, J.L. Alvarado, A.M. Jacobi, B.G. Jones, C.P. Marsh, *Appl. Phys. Lett.* **101**, 111605 (2012).
64. J.C. Love, L.A. Estroff, J.K. Kriebel, R.G. Nuzzo, G.M. Whitesides, *Chem. Rev.* **105**, 1103 (2005).
65. G.P. Lopez, H.A. Biebuyck, C.D. Frisbie, G.M. Whitesides, *Science* **260**, 647 (1993).
66. D. Mandler, I. Turyan, *Electroanalysis* **8**, 207 (1996).
67. N. Miljkovic, R. Enright, E.N. Wang, *ACS Nano* **6**, 1776 (2012).
68. K. Rykaczewski, *Langmuir* **28**, 7720 (2012).
69. S. Kim, K.J. Kim, *J. Heat Transfer* **133**, 081502 (2011).
70. M. AbuOrabi, *Int. J. Heat Mass Trans.* **41**, 81 (1998).
71. S. Anand, S.Y. Son, *Langmuir* **26**, 17100 (2010).
72. L. Cao, A.K. Jones, V.K. Sikka, J.Z. Wu, D. Gao, *Langmuir* **25**, 12444 (2009).
73. J.W. Rose, L.R. Glicksman, *Int. J. Heat Mass Trans.* **16**, 411 (1973).
74. R.D. Narhe, M.D. Khandkar, P.B. Shelke, A.V. Limaye, D.A. Beysens, *Phys. Rev. E* **80**, 031604 (2009).
75. C. Dietz, K. Rykaczewski, A.G. Fedorov, Y. Joshi, *Appl. Phys. Lett.* **97**, 033104 (2010).
76. N. Miljkovic, R. Enright, E.N. Wang, presented at the *3rd Micro/Nanoscale Heat & Mass Transfer International Conference* (Atlanta, GA, 2012).
77. M. Nosonovsky, B. Bhushan, *Ultramicroscopy* **107**, 969 (2007).
78. M. McCarthy, K. Gerasopoulos, R. Enright, J.N. Culver, R. Ghodssi, E.N. Wang, *Appl. Phys. Lett.* **100**, 1 (2012).
79. B. Bhushan, M. Nosonovsky, *Nano Lett.* **7**, 2633 (2007).
80. B. Bhushan, Y.C. Jung, *ACS Nano* **3**, 4155 (2009).
81. B. Pokroy, S.H. Kang, L. Mahadevan, J. Aizenberg, *Science* **323**, 237 (2009).
82. T.Q. Liu, W. Sun, X.Y. Sun, H.R. Ai, *Langmuir* **26**, 14835 (2010).
83. T.Q. Liu, W. Sun, X.Y. Sun, H.R. Ai, *Colloids Surf., A* **414**, 366 (2012).
84. N. Miljkovic, R. Enright, E.N. Wang, *J. Heat Transfer* (2012), in press.
85. J. Feng, Y. Pang, Z. Qin, R. Ma, S. Yao, *ACS Appl. Mater. Interfaces* **4**, 6618 (2012).
86. R. Enright, N. Dou, N. Miljkovic, Y. Nam, E.N. Wang, presented at the *3rd Micro/Nanoscale Heat & Mass Transfer International Conference* (Atlanta, GA, 2012).
87. C. Dietz, K. Rykaczewski, A. Fedorov, Y. Joshi, *J. Heat Transfer* **132**, 080904 (2010).
88. J.B. Boreyko, P.C. Collier, *ACS Nano* **7**, 1618 (2013)
89. K. Rykaczewski, J.H.J. Scott, S. Rajauria, J. Chinn, A.M. Chinn, W. Jones, *Soft Matter* **7**, 8749 (2011).
90. K. Rykaczewski, A.T. Paxson, S. Anand, X. Chen, Z. Wang, K.K. Varanasi, *Langmuir* **29**, 881 (2013).
91. K. Rykaczewski, J. Chinn, M.L. Walker, J.H.J. Scott, A. Chinn, W. Jones, *ACS Nano* **5**, 9746 (2011).

https://doi.org/10.1557/mrs.2013.103 Published online by Cambridge University Press

92. R.D. Narhe, W. Gonzalez-Vinas, D.A. Beysens, *Appl. Surf. Sci.* **256**, 4930 (2010).
93. D. Torresin, M.K. Tiwari, D. Del Col, D. Poulikakos, *Langmuir* **29**, 840 (2013).
94. J. Feng, Z.Q. Qin, S.H. Yao, *Langmuir* **28**, 6067 (2012).
95. X.T. Zhang, M. Jin, Z.Y. Liu, S. Nishimoto, H. Saito, T. Murakami, A. Fujishima, *Langmuir* **22**, 9477 (2006).
96. X.T. Zhang, M. Jin, Z.Y. Liu, D.A. Tryk, S. Nishimoto, T. Murakami, A. Fujishima, *J. Phys. Chem. C* **111**, 14521 (2007).
97. M. He, X. Zhou, X.P. Zeng, D.P. Cui, Q.L. Zhang, J. Chen, H.L. Li, J.J. Wang, Z.X. Cao, Y.L. Song, L. Jiang, *Soft Matter*, **8**, 6680 (2012).
98. Y. Nam, S. Sharratt, C. Byon, S.J. Kim, Y.S. Ju, *J. Microelectromech. Syst.* **19**, 581 (2010).
99. Y. Nam, Y. Sungtaek, *J. Adhes. Sci. Technol.* 1 (2012).
100. J.W. Rose, *Int. J. Heat Mass Trans.* **10**, 755 (1967).
101. J.B. Boreyko, Y.J. Zhao, C.H. Chen, *Appl. Phys. Lett.* **99**, 234105 (2011).
102. J. Cheng, A. Vandadi, C.L. Chen, *Appl. Phys. Lett.* **101**, 131909 (2012).
103. J.B. Boreyko, C.H. Chen, *Int. J. Heat Mass Transf.* **61**, 409 (2013).
104. X.H. Ma, X.D. Zhou, Z. Lan, Y.M. Li, Y. Zhang, *Int. J. Heat Mass Trans.* **51**, 1728 (2008).
105. J.W. Rose, *Int. J. Heat Mass Trans.* **23**, 539 (1980).
106. G.P. Thiel, J.H. Lienhard, *Int. J. Heat Mass Trans.* **55**, 5133 (2012).
107. H.C. Barshilia, A. Chaudhary, P. Kumar, N.T. Manikandanath, *Nanomaterials* **2**, 65 (2012).
108. G. Azimi, R. Dhiman, H.K. Kwon, A.T. Paxson, K.K. Varanasi, *Nat. Mater.* (2013), doi: 10.1038/nmat3545.
109. A. Lafuma, D. Quéré, *Europhys. Lett.* **96**, 56001 (2011).
110. T.S. Wong, S.H. Kang, S.K.Y. Tang, E.J. Smythe, B.D. Hatton, A. Grinthal, J. Aizenberg, *Nature* **477**, 443 (2011).
111. S. Anand, A.T. Paxson, R. Dhiman, D.J. Smith, K.K. Varanasi, *ACS Nano* **6**, 10122 (2012).
112. P. Kim, T.S. Wong, J. Alvarenga, M.J. Kreder, W.E. Adorno-Martinez, J. Aizenberg, *ACS Nano* **6**, 6569 (2012).
113. P.W. Wilson, W. Lu, H. Xu, P. Kim, M.J. Kreder, J. Alvarenga, J. Aizenberg, *Phys. Chem. Chem. Phys.* **15**, 581 (2013).
114. A.K. Epstein, T.S. Wong, R.A. Belisle, E.M. Boggs, J. Aizenberg, *Proc. Natl. Acad. Sci. U.S.A.* **109**, 13182 (2012).
115. D.J. Smith, R. Dhiman, S. Anand, E. Reza-Garduno, R.E. Cohen, G.H. McKinley, K.K. Varanasi, *Soft Matter* **9**, 1772 (2013).
116. A. Tuteja, W.J. Choi, G.H. McKinley, R.E. Cohen, M.F. Rubner, *MRS Bull.* **33**, 752 (2008).
117. X. Deng, L. Mammen, H.J. Butt, D. Vollmer, *Science* **335**, 67 (2012).
118. S. Nishimoto, B. Bhushan, *RSC Adv.* **3**, 671 (2013).
119. X.J. Liu, Y.M. Liang, F. Zhou, W.M. Liu, *Soft Matter* **8**, 2070 (2012).
120. D. Stokes, *Principles and Practice of Variable Pressure/Environmental Scanning Electron Microscopy (VP-ESEM)* (New York, Wiley, 2008).
121. N.A. Stelmashenko, J.P. Craven, A.M. Donald, E.M. Terentjev, B.L. Thiel, *J. Microsc.* **204**, 172 (2001).
122. M.P. Rossi, Y. Gogotsi, K.G. Kornev, *Langmuir* **25**, 2804 (2009).
123. N. Miljkovic, R. Enright, S.C. Maroo, H.J. Cho, E.N. Wang, *J. Heat Transfer* **133**, 080903 (2011).
124. N. Miljkovic, R. Enright, E.N. Wang, *J. Heat Transfer* **134**(8), 080902 (2012).
125. Z. Barkay, *Appl. Phys. Lett.* **96**, 183109 (2010).
126. B. Bhushan, Y.C. Jung, *J. Microsc.* **229**, 127 (2008).
127. K. Rykaczewski, J.H.J. Scott, *ACS Nano* **5**, 5962 (2011).
128. K. Rykaczewski, J.H.J. Scott, A.G. Fedorov, *Appl. Phys. Lett.* **98**, 093106 (2011).
129. S. Wiedemann, A. Plettl, P. Walther, P. Ziemann, *Langmuir* **29**, 913 (2013).
130. K. Rykaczewski, T. Landin, M.L. Walker, J.H.J. Scott, K.K. Varanasi, *ACS Nano* **6**, 9326 (2012). □



https://doi.org/10.1557/mrs.2013.103 Published online by Cambridge University Press